THE ASTROPHYSICAL JOURNAL, 479:222–230, 1997 April 10

THE VARIABILITY AND SPECTRUM OF NGC 5548 IN THE EXTREME ULTRAVIOLET

H. L. MARSHALL[1] AND T. E. CARONE[2]
Eureka Scientific, Inc., 2452 Delmer Street, Suite 100, Oakland, CA 94602; hermanm@usa1.com
B. M. PETERSON
Department of Astronomy, Ohio State University, 174 West 18th Avenue, Columbus, OH 43210
J. CLAVEL
ISO Observatory, ESA, Apartado 50727, 28080-Madrid, Spain
D. M. CRENSHAW
Computer Sciences Corporation, Laboratory for Astronomy and Solar Physics, NASA Goddard Space Flight Center, Code 681, Greenbelt, MD 20771
K. T. KORISTA
Department of Physics and Astronomy, University of Kentucky, Lexington, KY 40506
G. A. KRISS AND J. H. KROLIK
Department of Physics and Astronomy, Johns Hopkins University, Baltimore, MD 21218
M. A. MALKAN
Department of Astronomy, University of California, Math-Science Building, Los Angeles, CA 90095
S. L. MORRIS
Dominion Astrophysical Observatory, 5071 West Saanich Road, Victoria, BC, V8X 4M6, Canada
P. T. O'BRIEN
Department of Physics and Astronomy, University of Leicester, University Road, Leicester, LE1 3RH, UK
AND
G. A. REICHERT
Universities Space Research Association, NASA/Goddard Space Flight Center, Code 668, Greenbelt, MD 20771
Received 1996 March 12; accepted 1996 October 29

ABSTRACT

We have measured the light curve and spectrum of NGC 5548 obtained with the *Extreme Ultraviolet Explorer* (*EUVE*) during a period when the galaxy was also intensively monitored with the *Hubble Space Telescope*, the *International Ultraviolet Explorer*, and ground-based telescopes. NGC 5548 was observed with *EUVE* for a total of about 20 days spread over a period of 2 months. The broadband extreme ultraviolet (EUV) light curve showed several factor of 2 variations on 0.5 day timescales and one factor of 4 decrease over 2 days. The normalized variability index was smaller than in the *EUVE* observation of Mrk 478. Cross-correlation of the EUV light curve with the contemporaneous ultraviolet light curve indicates that the EUV and UV/optical variations are, to within the limitations of these data, simultaneous, although the amplitude in the EUV is twice that in the UV.

The shape of the *EUVE* spectrum is consistent with a gradual steepening from the UV through the soft X-rays. Contrary to reports by others, we do not detect any emission lines in the EUV spectrum that would arise in optically thin spectral models. We believe that the reported line detections were, in fact, due to a low-level fixed pattern in the detector background. Models of the spectrum may be constrained by the time-averaged flux in the broadband detector combined with the weakly constrained spectral shape. A thermal model best describes the *EUVE* spectrum and its variations.

Subject headings: galaxies: active — galaxies: individual (NGC 5548) — galaxies: Seyfert — ultraviolet: galaxies

1. INTRODUCTION

Coordinated continuum and emission-line variability has proven to be a useful probe of the nature of the broad emission-line region in active galactic nuclei, as well as of the continuum-emitting region itself (see Peterson 1993 for a review). However, a significant weakness of variability monitoring programs that have been undertaken to date is that the continuum information has been available only at wavelengths longward of Lyα λ1216, whereas the emission lines are driven predominantly by the continuum shortward of the Lyman limit. Study of the variation of the ionizing continuum itself is of key importance in deciphering the meaning of the continuum–emission-line time delays and in understanding the relative amplitude of variability of the lines and continuum (which provides information about the reprocessing physics). Furthermore, as pointed out by Krolik et al. (1991), Collin-Souffrin (1991), and Courvoisier & Clavel (1991), the apparent lack of phase differences between the continuum variations observed at different wavelengths places a severe constraint on which sorts of signals may coordinate fluctuations in accretion disk models or indeed in any thermal model with a radial temperature gradient.

Here we report on an extended *Extreme Ultraviolet Explorer* (*EUVE*) observation of the Seyfert 1 galaxy NGC 5548 that was obtained in connection with a large multi-

[1] Present address: 5 Whipple Road, Lexington, MA 02173.
[2] Also Space Sciences Laboratory, University of California, Berkeley, CA 94720.

wavelength campaign to monitor the continuum and emission-line fluxes in 1993, previously reported by Korista et al. (1995). One of the key findings of that experiment is that the variations in the UV (1350 Å) and optical (5100 Å) are simultaneous to within the uncertainties imposed by the sampling, i.e., to within ~ 1.2 days at 90% confidence. The *EUVE* observations reported here were obtained to measure *directly* the relationship between the *ionizing continuum* and the longer wavelength continuum and the emission lines.

The only other active galaxy that has been observed by *EUVE* with similar exposure time was Mrk 478 (Marshall et al. 1996, hereafter Paper I). During that *EUVE* observation Mrk 478 showed large EUV flux variations, and its EUV spectrum showed no emission lines. The data are consistent with a model where the EUV flux comes from the Wien tail of a blackbody or accretion disk spectrum, so that small temperature variations can cause large changes in the EUV count rates. Only small changes in the UV fluxes would be expected in this model, because the UV originates in the Rayleigh-Jeans portion of a blackbody spectrum. In the case of Mrk 478, there were no simultaneous observations of the emission lines or the UV or X-ray continua, so the model could not be critically tested.

2. OBSERVATIONS

2.1. *General*

NGC 5548 was observed in three contiguous sections in 1993 March–May from TJD ($\equiv$JD$-$2440000) 9057.3 to 9070.6, 9104.0 to 9111.8, and 9119.6 to 9121.9. It was observed 0.°3 off-axis, which is optimal for highly absorbed targets such as active galactic nuclei because the spectrum can be extended to shorter wavelengths than is possible on-axis. This technique was first suggested for use in observing Mrk 478 (Paper I) because the spectrum is shifted away from the detector edge, which limits the short-wavelength end of the spectrum, and systematic errors are reduced.

During this same time period, *International Ultraviolet Explorer* (*IUE*) spectra were obtained once every 2 days between TJD 9060.6 and 9134.5, and *Hubble Space Telescope* (*HST*) FOS spectra were obtained daily between TJD 9097.0 and 9135.1. Less regularly sampled ground-based observations were also made during this time period. All of these data are described by Korista et al. (1995).

2.2. *Deep Survey Light Curve*

The deep survey (DS) data were reduced in the same manner as for Mrk 478 (Paper I) except that the DS dead spot (Sirk 1994) was not a problem, another advantage of off-axis observations. Briefly, the method involves using a likelihood method (described in Marshall 1997) that uses the DS point-spread function. The effective exposure time was determined by numerically integrating the detector fractional live time, multiplied by the fraction of the processed events that were delivered to the telemetry stream, and the ratio of the telescope throughput at 0.°3 off-axis to the on-axis value. The first two corrections are known as the dead-time and "Primbsch" corrections and are supplied by the standard *EUVE* processing, and the third is the vignetting correction determined from the vignetting map supplied by the *EUVE* project. These effects are described in detail in the *EUVE* Guest Observer Data Products Guide (Miller-Bogwell & Abbott 1995).

The time intervals of good data were limited to times when the DS telescope boresight was less than 102° from the local orbital zenith. This criterion is applied so that the atmosphere attenuates less than 5% of the light at 120 Å (determined by integrating a path through a model of the Earth's atmosphere). The total detector ON time was 580,726 s, but the total effective time was 474,258 s. The count rates were estimated in three-orbit bins, where an orbit is 96 minutes. Shorter time bins are possible, but the count rate is not observed to vary so rapidly. The live time per orbit varies as the spacecraft enters daylight or the South Atlantic Anomaly when the background rates are so high that the detector high voltage may be turned down. Thus, the average exposure per orbit is about 15 minutes, and the average exposure in each bin is about 3000 s.

The light curve is shown in Figure 1. The average count rate, $\bar{R}$, was 0.059 ± 0.002 counts s^{-1} over the entire time period. Using the value of $N_{\rm H}$ for NGC 5548, 1.65×10^{20} cm^{-2} (based on a private communication from Lockman cited by Nandra et al. 1993, hereafter N93), and an assumed power-law (PL) spectrum with slope 0–2 ($f_\nu \propto \nu^{-\alpha}$), then the effective wavelength of the bandpass is about 76 Å, the spectral density at this wavelength is 135 μJy, and the flux in the 70–90 Å bandpass is about 8.0×10^{-13} ergs cm^{-2} s^{-1} and is not strongly model-dependent. The models applied in § 3 produce similar fluxes.

The first contiguous section of the light curve shows several flux changes by a factor of 2 over timescales of 1–2 days and a factor of 4 variation from peak to minimum. One gets the overall impression that this source is less variable than Mrk 478 (Paper I), however. To quantify this impression, we computed the normalized standard deviation. Briefly, this quantity, ξ, is just the ratio of the dispersion to the mean in a model of the light curve that assumes that the fluxes are merely samples of a Gaussian distribution of true intensities. The likelihood function that is maximized to determine the mean and dispersion is the product of the probabilities of obtaining each observed count rate, given that the true intensity is unknown. The uncertainty in the dispersion is easily determined from the likelihood function by standard methods (see Lampton, Margon, & Bowyer 1976). For NGC 5548, $\xi = 0.273 \pm 0.023$, while $\xi = 0.408 \pm 0.031$ for Mrk 478, confirming the impression that the EUV flux of NGC 5548 is less variable than that of Mrk 478. This method does not account for correlations of the source fluxes, so this result could be more an indication that the timescale for variation of NGC 5548 is longer than that of Mrk 478.

2.3. *Spectrometer Observations*

The image of the short-wavelength spectrometer is shown in Figure 2. Time intervals were chosen such that the detector count rate was never above 50 counts s^{-1}, which is a rate at which corrections to the data for detector dead time and Primbsching are larger than 5%, so these corrections were not applied to the exposure times. As with the DS data, there is also a selection on the direction of the telescope boresight. We determined that restricting the data in this way reduces the background by a total of 25% and the total time by 11%, resulting in a net improvement of 7.5% in the signal-to-noise ratio (SNR). The resultant total detector ON time was 558,549 s (out of a possible 629,600 s).

The extracted spectrum was somewhat sensitive to the details of the background and aperture selection, as a result

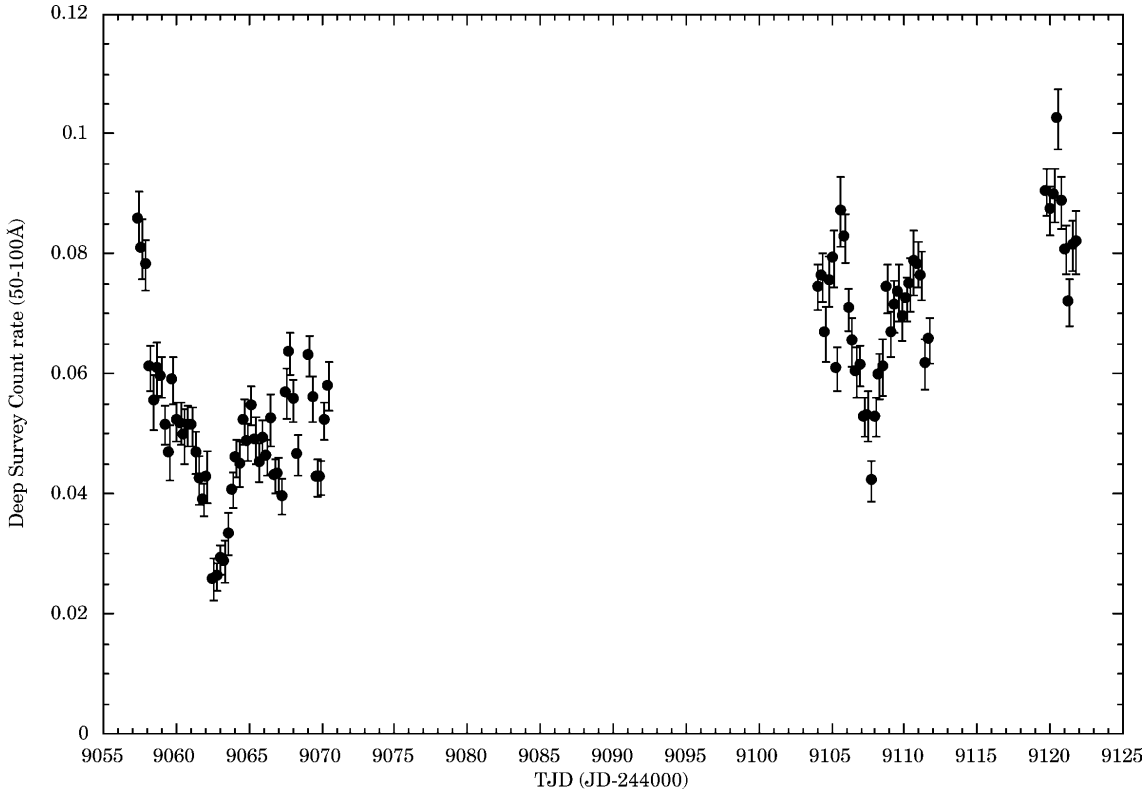

FIG. 1.—Time history of the NGC 5548 count rate obtained by the *EUVE* Deep Survey (DS) imaging detector averaged over 3 orbit intervals

of the poor statistics and the fixed pattern noise (see below for further discussion), so a simple 10 pixel wide rectangular source aperture and two 30 pixel wide background apertures (with near edges 11 pixels from spectrum center) were established. The background apertures are placed on opposite sides of the source aperture, so the background estimation is relatively insensitive to the background gradient. Below 70 Å, which is very near the detector edge (see Fig. 2), the background is very large relative to any possible source flux, and it curves with the side of the detector, so the background subtraction is dominated by systematic and statistical errors. A new effective area curve was derived specifically for observations made at 0°.3 off-axis such as this one and will be presented elsewhere (Marshall & Dupuis 1997).

The image shows that these data do not define the spectral shape well. Furthermore, we find no compelling evidence for the presence of emission lines, as claimed by Kaastra, Roos, & Mewe (1995). To quantify this conclusion, we performed several tests. First, we examined the background in detail to see if background structure could account for irregularities in the spectrum that might be interpreted as real features. We found that there is a low-level pattern in the background that appears as a series of stripes angled at 7°.5 counterclockwise from horizontal. This pattern has a period of about 15 pixels and an amplitude of about 5% of background over the 70–100 Å region, in which the background increases systematically with decreasing wavelength from 52 to 99 counts $Å^{-1}$ $pixel^{-1}$.[3] The projected period is 115 pixels in the wavelength direction, or 7.75 Å.

For the extraction aperture size of 10 pixels in the imaging direction, the ripple has an average amplitude of 37.5 counts $Å^{-1}$, while the average in the spectrum is only 27 counts $Å^{-1}$. Because the ripple is tilted with respect to the spectral dispersion, an over- or undersubtraction of the background can occur when estimating the background from opposite sides of the spectrum, depending on whether the spectrum falls on a valley or a peak of the ripple. The ripple amplitude is strongest at the short-wavelength edge of the detector, indicating that it is a quantum efficiency variation responding to the scattered Lyα light. This effect is the most significant cause of systematic error in the extracted spectrum and the result of the extraction was somewhat sensitive to the exact choice of background regions. We chose two regions 30 pixels wide in the imaging direction on either side of the source spectrum, separated by 10 pixels from the center of the dispersion line.

The extracted spectrum is shown in Figure 3. There is a systematic background subtraction error that appears right at the edge of the detector, at a wavelength of 65 Å, where the bright rim is difficult to subtract properly, so only the 70–100 Å portion of the spectrum is shown. Furthermore, no net signal was detected in the 100–170 Å region where the spectrum is severely absorbed by the Galactic interstellar medium (ISM). The effects of the fixed pattern noise are apparent as peaks in the net spectrum at a period of about 8 Å with corresponding troughs at 72 and 80 Å. Attempts to model the spectrum were frustrated by this systematic error. In a similar inconsistency in the data, the measured flux in the 70–90 Å bandpass is $2.9 \pm 1.5 \times 10^{-13}$

[3] In this context, pixels are defined in the original coordinate system of the spectral image, which is 2048 square. Thus, the dimension of a pixel is about 0.065 Å long in the x direction and 0°.0012 in the y direction.

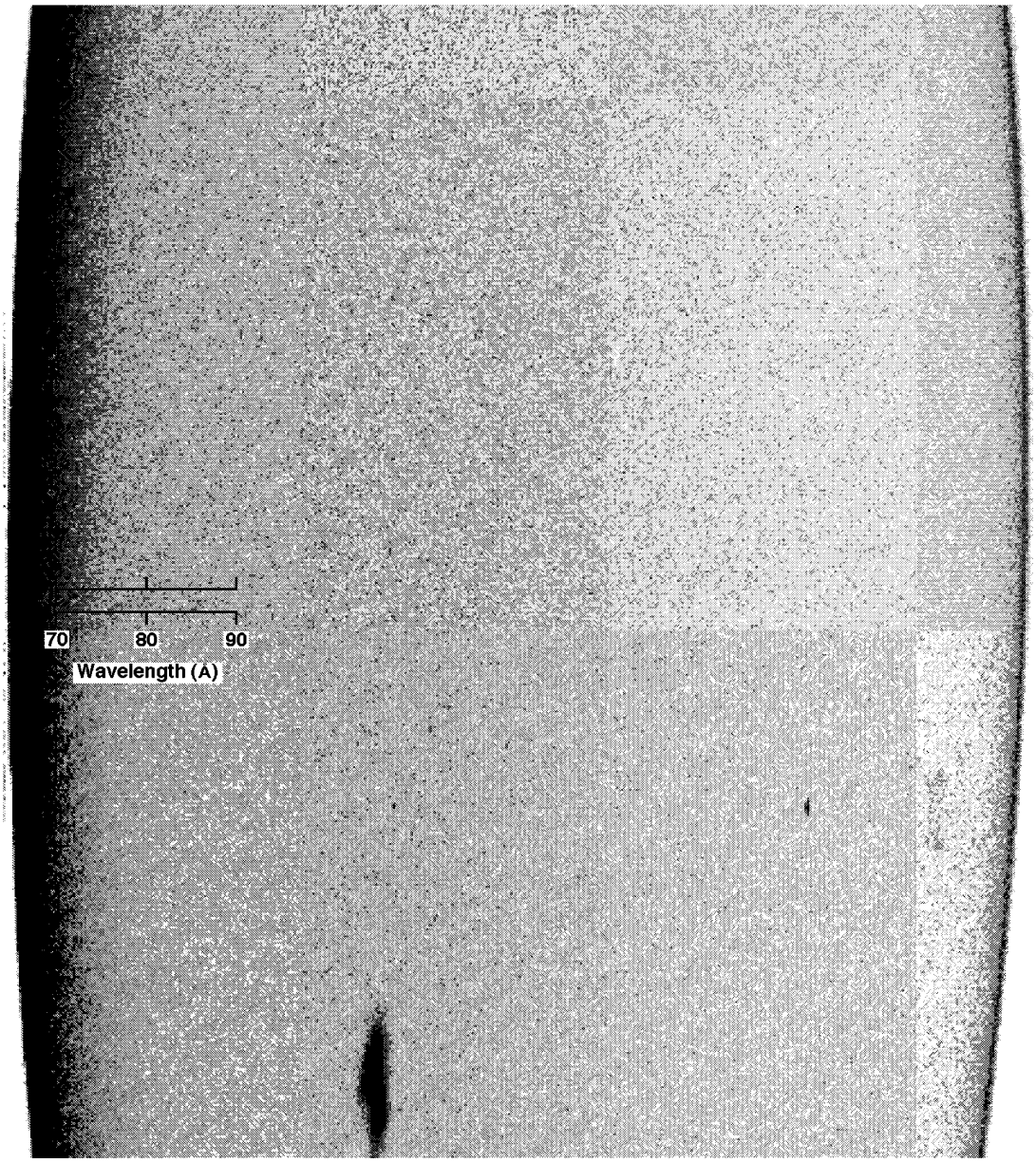

FIG. 2.—Spectral image of NGC 5548 using the *EUVE* short-wavelength spectrometer data using the entire data set from 1993. The dispersion direction is horizontal and the vertical direction is an imaging coordinate. The spectrum should appear near the center left portion of the detector. If there were any emission lines, they would appear as vertically elongated blobs of events. There is a low-level background pattern that appears as ripples running at a 27° angle from horizontal toward the upper right. A hot region is visible along the lower edge as well as two weaker hot spots. The image was compressed horizontally; otherwise, the detector edge would appear circular and the angle of the background pattern to the horizontal would be 7°.5. Enhanced background resulting from scattered Lyα is visible at the left detector edge.

ergs cm^{-2} s^{-1}, a factor of 2.7 lower than that inferred from the DS count rate. We suspect that the systematic background subtraction error in the 70–75 Å region is responsible for this discrepancy (as suggested by the modeling results from § 3).

The variance of the estimated background is increased over the value expected solely from Poisson statistics. The exact value of the excess variance depends strongly on wavelength, however, because it is related to the background that decreases rapidly with distance from the short-wavelength edge of the detector. Taking regions 5 Å by 100 pixels on both sides of the spectrum, we find that the variance is 2.38, 1.16, and 1.01 times the expected value at 70, 75, and 80 Å, respectively. All statistical errors that we quote have been increased appropriately to account for this unidentified noise source. This excess variance must be included in χ^2 calculations; otherwise, acceptable models will be erroneously rejected. The effect may account for the poor χ^2 value for the PL model of Mrk 478 (Paper I).

The second test involved collapsing the spectral image along the dispersion direction, so as to obtain the best SNR for detecting a continuum source. If detected, the projected image would give an accurate position for the source, in case there were attitude errors or residual distortions in the detector. A very weak source was found centered at y location 1014.7 and totaling 0.00117 ± 0.00021 counts s^{-1} in

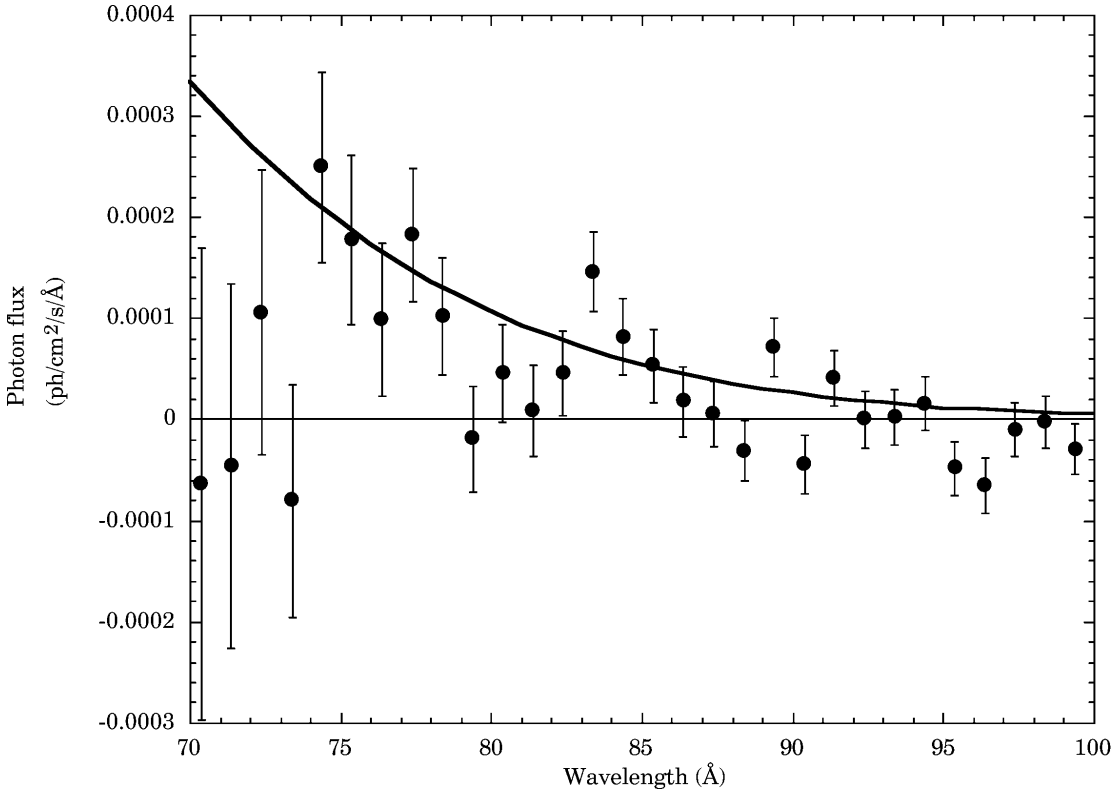

FIG. 3.—Soft X-ray spectrum of NGC 5548 taken with *EUVE*. The uncertainties were derived from the variance of the data adjacent to the spectral extraction region and are somewhat larger than Poisson uncertainties, especially at short wavelengths. Only the 70–100 Å region is shown, which is not affected by the detector edge subtraction errors; no net signal is observed longward of 100 Å. Note that no emission lines are apparent. All data from the 1993 observations were used in deriving the spectrum. *Bold line:* Predicted spectrum from model C (see table 1).

the 70–90 Å region for a 5.5 σ detection. Thus, we are confident that the target was detected in the spectrometer detector.

In order to search for possible emission at 90 Å, we extracted a 2 Å wide profile along the imaging direction. We found 28 ± 35 counts in a 10 pixel region in the imaging direction, after subtracting background (derived, as before, from averaging two regions of 30 pixels wide on either side of the source). Thus, contrary to the results of Kaastra et al. (1995), we find no evidence for a 90 Å emission line. Although Kaastra et al. claim to detect a line at 70 Å as well, this region is strongly affected by systematic background subtraction errors and makes a poor choice for testing the hypothesis that there are significant emission lines in the EUV spectrum of this source.

Kaastra et al. (1995) generated a spectrum only for the 1993 March data subset, so we have examined this subset in detail as well. The total exposure time is 332,481 s, while our more restrictive data selection gives 292,273 s, again improving the SNR by eliminating high-background periods. As before, we find no evidence for emission lines: the observed count in a 10 pixel high aperture centered on the source in the 90 ± 0.5 Å region is 319, while the expected count is 345 from background. The net signal is also negative in a 2 Å band. We note, however, that Kaastra et al. used an extraction region centered on pixel 1024 (Kaastra 1996, private communication), so their 9 pixel aperture does not overlap ours. A new spectral observation was recently obtained, so we hope to resolve the issue using the new data. The new observations have been dithered in such a way to eliminate the effect of the ripples, so background subtraction should not be a problem.

3. MODELING THE EUV SPECTRUM

Because of the poor detection and the dominance of systematic errors, no formal fits to the short-wavelength data were performed. We instead checked the spectral models previously fitted to Position Sensitive Proportional Counter (PSPC) data (N93 and Walter et al. 1994, hereafter W94). Both groups found that pure PL spectral fits were unacceptable, so that a soft component was indicated. The best N93 fits included an edge at about 0.8 keV, but this is well outside the range of the *EUVE* spectra, so we will concentrate on the extrapolation of the models to 0.1 keV, which are sensitive to the model of the soft excess. For our purposes, the EUV spectrum can be modeled locally as a PL because the effective bandpass is narrow, limited to 75 Å on one side by the telescope mirror reflectivity and to about 90 Å on the other side by the ISM attenuation. Therefore, we can approximate all the models with PL spectra that are valid only for a small portion of the soft X-ray band.

Model A, a pure PL model from N93 (see their Table 4), is a simple model, but they showed that this model does not fit the *ROSAT* PSPC data, even when an absorption edge (outside of the *EUVE* band) is added to reduce the residuals significantly. Model B is their best-fit PL model that includes a blackbody component; again, N93 added an absorption edge at O Kα to get a good fit. Model C was taken from W94 (their description A), where the spectrum is assumed to take a PL shape from the UV with a slope determined from the UV data, an exponential cutoff in the EUV, and an additional PL component that matches the *Ginga* hard X-ray spectrum. Model D was taken from description B of W94, where the spectrum is a PL with an

TABLE 1

POWER-LAW APPROXIMATIONS FOR SEVERAL SPECTRAL MODELS

Model	Soft Excess	Reference	PSPC Rate (counts s^{-1})	A (μJy at 0.15 keV)	α	N_H (10^{20} cm^{-2})
A.....	None	Nandra et al. 1993	1.78	23.4	0.98	1.65
B.....	BB[a]	Nandra et al. 1993	1.78	20.1	0.6	1.65
C.....	Cutoff PL[b]	Walter et al. 1994	3.27	105	1.25	1.93
D.....	Cutoff PL[c]	Walter et al. 1994	3.27	150	2.14	1.93

[a] The blackbody model parameters are taken from Table 4 of N93: $kT = 0.060$ keV and $A_2 = 0.039$ photons cm^{-2} s^{-1} keV^{-1}. Adding this component to their PL component gives a shape with the PL spectral parameters given in the table.

[b] Parameters were derived from a fit to the unabsorbed spectrum from 0.1 to 1.0 keV in their Fig. 2*a*.

[c] Parameters were derived from a fit to the unabsorbed spectrum from 0.15 to 0.4 keV in their Fig. 2*b*.

energy index fixed at 0.3 in the UV and is otherwise identical to model C. The cutoff in model C is at a much higher energy (0.415 keV) than in model D (0.067 keV), so the intrinsic spectrum is much steeper in the EUV band in model D than in the other three models. Parameters for these PL descriptions are summarized in Table 1.

Due to significant variations in the soft X-ray flux, we attempt to normalize the models to the current data set. The count rates in the *ROSAT* PSPC are well known for the N93 and W94 observations (see Table 1) but there was no PSPC observation within a month of our *EUVE* observations. We have chosen to normalize the models to the average count rate observed during the several months prior to our observations (TJD 8750–9020). The PSPC count rate varied between 3.9 and 12.2 counts s^{-1}, with an average of 6.75 counts s^{-1}, according to the *ROSAT* consortium catalog available from the HEASARC. The predicted DS count rates and SW photon fluxes are shown in Table 2.

Formally, model C (description A from W94) gives the best agreement with all the observed fluxes. Its main disagreement is in the 70–75 Å band (a 2 σ difference), where all models overpredict the flux. However, due to possible systematic background subtraction errors mentioned earlier (see § 2.3), this may not be a significant problem.

This model involves a PL shape that matches the UV slope but is cut off in the EUV with a cutoff energy of 415 eV (W94). The models mainly differ in the magnitude of the EUV flux predicted, relative to the X-ray band, and not in the spectral shape in the EUV band.

The *EUVE* data provide us with one of the best observations of the ionizing continuum ever obtained for an active galaxy. From the UV bands observed by *IUE* down through the soft X-rays observed by *ROSAT*, the ionizing continuum is described by a *gradually* steepening slope. The continuum slope in the mid-UV is slightly flatter than -1 and steepens to approximately -1 at the short-wavelength end of the short-wavelength prime (SWP) camera (around 1200 Å). The continuum beyond Lyα gradually steepens to hit the observed *EUVE* flux level, with an *IUE*-to-*EUVE* slope averaging -1.15. To reach the observed soft X-rays the slope must continue steepening to -1.3, which is consistent with the flux level and spectral slope measured by *ROSAT* (according to models C or D). The slope measured within the *EUVE* bandpass is also consistent with this gradual steepening. This gradually steepening ionizing continuum we deduce for NGC 5548 is almost identical to the "hard" model hypothesized in Krolik et al. (1991) and probably describes the spectra of many other Seyfert 1 nuclei as well.

4. COMPARISON OF THE EUV AND UV LIGHT CURVES

Our primary goal is to measure any possible phase delay between the EUV and UV continuum variations. Unfortunately, the EUV and UV data are not exceedingly well matched for this purpose: the EUV continuum is well sampled on very short timescales but broken up on timescales of weeks. Relative to the EUV data, the UV observations, by contrast, are poorly sampled on timescales shorter than 1 day but are better sampled over longer intervals. Close comparison of the light curves shows that only the second set of *EUVE* observations, those obtained in the range $9104.0 \leq \mathrm{TJD} \leq 9111.8$, can be quantitatively compared with the UV observations obtained by *HST*. During the first set of EUV measurements, the UV continuum was poorly sampled and with *IUE* only, so the UV continuum errors are relatively large. Moreover, one *IUE* observation during this time is underexposed and had to be discarded, as described by Korista et al. (1995). The third set of EUV observations was too brief to carry out a meaningful comparison. Fortunately, significant continuum variations were detected in both the EUV and UV bands during the second set of observations, as shown in Figure 4, and indeed it is clear that the variations are nearly in phase, *provided that*

TABLE 2

PREDICTIONS FROM SPECTRAL MODELS COMPARED TO *EUVE* DATA

Model	DS Rate (10^{-3} count s^{-1})	SW Spectrometer (10^{-5} photons cm^{-2} s^{-1} $Å^{-1}$)			
		70–75 Å	75–80 Å	80–85 Å	85–90 Å
A.....	35.2	17.0	10.4	6.0	3.2
B.....	30.8	15.0	9.0	5.1	2.8
C.....	52.6	27.3	15.6	8.3	4.1
D	68.5	34.4	20.8	11.7	6.2
Observed.....	59 ± 2	5.4 ± 9.8	10.0 ± 3.1	6.8 ± 1.9	2.3 ± 1.4

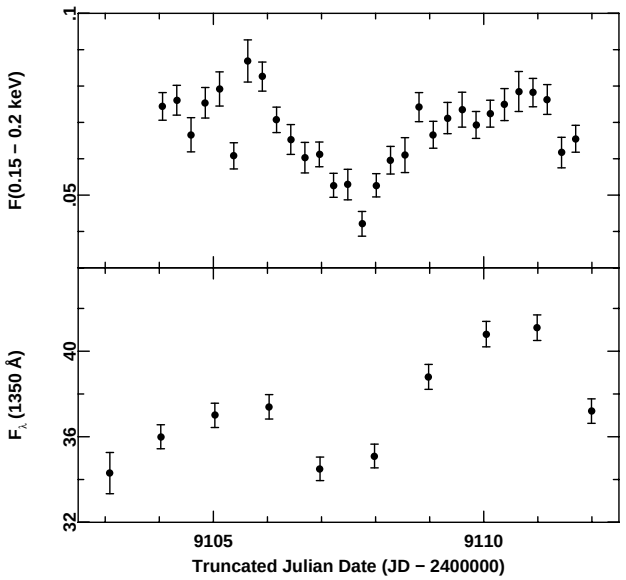

FIG. 4.—*Upper panel*: EUV DS count rates as a function of time during the second set of observations shown in Fig. 1. *Lower panel*: Simultaneous 1350 Å fluxes, from Korista et al. (1995).

aliasing is not a problem. The amplitude of variability, which can be simply characterized by the ratio of maximum to minimum flux $R_{\max}$ or by the rms variations about the mean $F_{\rm var}$ (Clavel et al. 1991), is about twice as large in the EUV band ($R_{\max} = 2.064$, $F_{\rm var} = 0.138$) as in the UV band ($R_{\max} = 1.198$, $F_{\rm var} = 0.060$) during this period.

The phase difference between the two light curves can be quantified by cross-correlation of the light curves shown in Figure 4. The cross-correlation function (CCF) was computed in two ways, by using the interpolation method of Gaskell & Sparke (1986) and the discrete correlation function (DCF) method of Edelson & Krolik (1988), with both algorithms as implemented by White & Peterson (1994). The results are shown in Figure 5.

If we assume that any structure in the CCF on timescales shorter than we sampled is unimportant, the centroid of the CCF gives an order of magnitude estimator of any relative delay between the two light curves. It is $\tau_{\rm cent} = -0.096$ days, i.e., the UV variations apparently *precede* the EUV variations by a very small amount.

In an attempt to assess the uncertainty in this result, Monte Carlo simulations similar to those described in more detail by Korista et al. (1995) were carried out. In these simulations, we make the simple assumption that the UV light curve shows the same variations as we observed in the EUV continuum, but with a known lag. If the true time relationship between the two light curves is more complicated (e.g., there is a "transfer function" relating one to the other, but it is not simply a δ function), the uncertainty in the characteristic lag we infer will be subject to a systematic error, the magnitude of which depends on the details of that relationship. We then carry out repeated simulations to find the largest lag that is in a statistical sense consistent with the observed value of $\tau_{\rm cent}$. For each Monte Carlo realization, we start with the observed EUV light curve as in Figure 4 and alter the fluxes with random Gaussian deviates that are consistent with the typical measurement errors. This revised EUV light curve is then resampled onto a

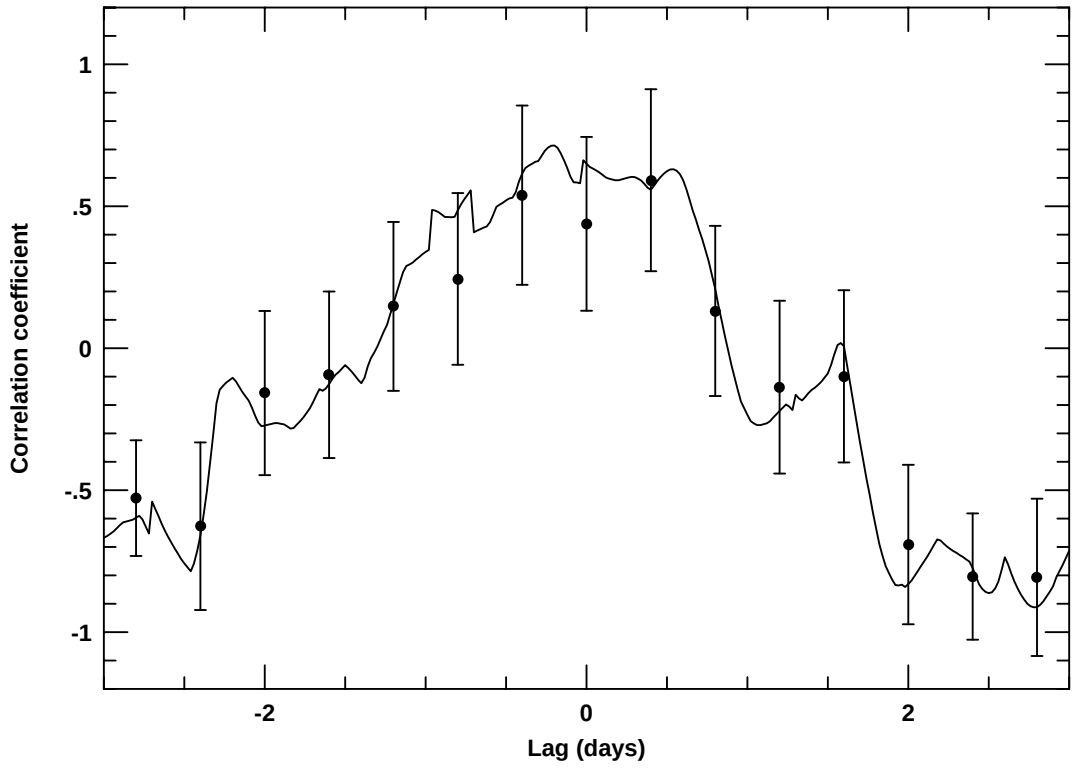

FIG. 5.—Cross-correlation functions (CCFs) produced from the light curves in Fig. 4. A positive lag corresponds to a delay of the UV variations relative to the EUV variations. The solid line is the interpolation CCF and the filled circles with error bars show the corresponding DCF values.

linear grid and time shifted by a given amount to serve as the model for the UV continuum. The model UV light curve is generated through a linear equation that dilutes the UV variations in amplitude to be consistent with the observed level of variability of the UV continuum. The model UV light curve is then sampled in the same pattern as the FOS observations, but with the initial point allowed to vary at random within ± 0.5 days of the true starting point. Random Gaussian deviates that are consistent with the uncertainties in the FOS data are then applied to the sampled data. The revised EUV light curve and the final model UV light curve are then cross-correlated as though they were real data, and the value of $\tau_{\rm cent}$ is determined. After many such realizations (usually 500), the recorded values build up a cross-correlation peak distribution (CCPD; Maoz & Netzer 1989) that can be used in statistical tests. The rms widths of the CCPDs so determined are typically around 0.22 days for model lags near zero. By performing several such simulations, we find that for model lags larger than 0.25 days, the probability of obtaining our experimental result $\tau_{\rm cent} = -0.096$ days drops to below 10%. Thus, based on these simulations, we tentatively conclude that the UV lags behind the EUV by no more than 0.25 days at 90% confidence. This may be compared with the analogous 90% confidence upper limit on the UV/optical lag of 1.2 days found by Korista et al. (1995).

We note, however, that this upper limit is only valid to the extent that the underlying assumptions are realistic. If the UV and EUV light curves are not merely copies of one another with a mutual lag, the simulations do not provide a relevant error estimate. Nonetheless, it is clear from the "raw" CF that any characteristic delay in this data set cannot be greater than $\simeq 1$ day. We also reiterate our earlier comment about the dangers of aliasing resulting from the short duration of the experiment; these data do not allow us to search for correlations at lags larger than ~ 4–5 days. Indeed, if we attempt to compute the CCF using *all* of the available EUV and UV continuum points, we find that there is a secondary peak at a lag of ~ 5 days. It is conceivable that a longer and more continuous run of data might reveal other peaks, but for the time being we pursue the hypothesis that the strong correlation at small lags displayed here is real.

One empirical result is immediately evident from these variability data. Krolik et al. (1991) claimed that the amplitude of variations increases with observing frequency, from the optical through the UV. Others have questioned whether the *nuclear nonstellar* continuum really does become harder when it brightens, because a sufficiently large contribution of (red, nonvariable) starlight could artificially mimic such an effect. Fortunately, the starlight contributions to the *IUE* SWP and *EUVE* fluxes are negligible, so these data confirm the previous result that the continuum hardens as it brightens. Taken together with the observations of Mrk 478 (Paper I), we suggest that this behavior may be common for the optical-EUV continua of Seyfert 1 nuclei.

5. DISCUSSION

The lack of significant emission lines and the rapid variability (see Paper I and Elvis et al. 1991) both argue against optically thin models of the EUV flux in this active galaxy. Thus we are led to consider optically thick continuum models of the EUV flux.

The EUV variability is significantly greater than that in the UV (a factor of 2 in the EUV compared to a change of less than 10% in the UV, as seen in Fig. 4), making it difficult to connect these bands with the simple cutoff PL spectrum in model C. The EUV point is below the cutoff energy, so changing the cutoff dramatically could have the desired effect but only if it drops by an order of magnitude or so.

Model D decouples the EUV and UV variations well and provides an explanation for the significant difference in variations in the same manner as suggested for Mrk 478 (Paper I): the EUV flux could be measuring the Wien tail of a thermal spectrum (say, a hot accretion disk) while the UV flux is in the Rayleigh-Jeans portion. The EUV flux (as well as the *ROSAT* count rate) would be very sensitive to the temperature of this component, while the UV flux would not be. W94 determined that the EUV component should have a temperature of $kT = 0.07$ keV. Still, in order for this model to work, the UV light would have to be diluted, say by a PL spectral component that dominates the optical and near IR bands or the outer, cooler parts of the accretion disk. If 30% of the light at 1350 Å is due to the same thermal component that dominates the EUV, then 30% temperature fluctuations are allowable, which are sufficient to account for the $\times 2$ EUV count rate variations. If we associate the EUV component with a hot, thermally variable, inner region of an accretion disk, then the UV light would arise predominantly in the cooler, more stable, outer portions.

If the UV and EUV variations are *not* produced cospatially, then the small delay between the UV and EUV changes would require that the signal that coordinates the two bands must travel at least mildly relativistically. While we do not know the central mass in NGC 5548, estimates based on the assumption that the dynamics of the broad emission-line gas are dominated by the gravity of the central object and some accretion disk model fits give $M \sim 10^8\ M_\odot$ (Peterson 1987; Krolik et al. 1991; Wanders et al. 1995; Done & Krolik 1996). The corresponding *minimum* signal propagation speed is then $> 0.25 c M_8 (r_{\rm UV}/5r_g)(\Delta t_{\rm max}/0.25d)^{-1}$, where M_8 is the central mass in units of $10^8\ M_\odot$, $r_{\rm UV}/r_g$ is the radius of the region producing the 1350 Å continuum fluctuations measured in gravitational radii, and $\Delta t_{\rm max}$ is an upper bound on the characteristic time delay between the two bands.

The variability timescales are reasonable for accretion disk models. In virtually all thermal models for the continuum, the region that emits the higher frequency radiation is hotter and closer to the central object, so there is a generic expectation is that the higher frequency continuum should vary faster and more strongly. To be more specific, we consider the model for NGC 5548 described by Krolik et al. (1991). Roughly, it predicts that much of the EUV emission is coming from a radius about half that of the 1300 Å emitting region. In the simple accretion disk model illustrated in their Figure 8, the radius enclosing half of the 1300 Å continuum is $5r_g$ (for a black hole mass of $10^8\ M_\odot$), which accounts for the dilution required to match the EUV and UV variability amplitudes. The significantly larger variability amplitude of the EUV continuum implies that it is mostly emitted from the *innermost* disk radii, close to the smallest marginally stable orbit around the black hole, which is where the highest energy photons from an accretion disk would be expected to originate. Most of the varia-

tions we observe in the *IUE* and *EUVE* bands would then arise from instabilities in the innermost part of the disk.

This work has been supported by NASA through contract NAS 5-32485 to Eureka Scientific, Inc., a private corporation created to promote the active pursuit of scientific research, and through grant NAGW-3315 and Space Telescope Science Institute grant GO-3484.01-91A to Ohio State University. During the course of this work, we have made significant use of the HEASARC WWW browse capability.

REFERENCES

Clavel, J., et al. 1991, ApJ, 366, 64
Collin-Souffrin, S. 1991, A&A, 249, 344
Courvoisier, T. J.-L., & Clavel, J. 1991, A&A, 248, 389
Done, C., & Krolik, J. H. 1996, ApJ, 463, 144
Edelson, R. A., & Krolik, J. H. 1988, ApJ, 333, 646
Elvis, M., Giommi, P., Wilkes, B. J., & McDowell, J. 1991, ApJ, 378, 537
Gaskell, C. M., & Sparke, L. S. 1986, ApJ, 305, 175
Kaastra, J. S., Roos, N., & Mewe, R. 1995, A&A, 300, 25
Korista, K. T., et al. 1995, ApJS, 97, 285
Krolik, J. H., Horne, K., Kallman, T. R., Malkan, M. A., Edelson, R. A., & Kriss, G. A. 1991, ApJ, 371, 541
Lampton, M., Margon, B., & Bowyer, S. 1976, ApJ, 208, 177
Maoz, D., & Netzer, H. 1989, MNRAS, 236, 21
Marshall, H. L. 1997, AJ, submitted
Marshall, H. L., Carone, T. E., Shull, J. M., Malkan, M. A., & Elvis, M. 1996, ApJ, 457, 169 (Paper I)
Marshall, H. L., & Dupuis, J. 1997, in preparation
Miller-Bogwell, A., & Abbott, M. 1995, *EUVE* Guest Observer Data Products Guide (Washington: NASA)
Nandra, K., et al. 1993, MNRAS, 260, 504 (N93)
Peterson, B. M. 1987, ApJ, 312, 79
———. 1993, PASP, 105, 247
Sirk, M. 1994, internal *EUVE* memo MMS/*EUVE*/0084/94.
Walter, R., Orr, A., Courvoisier, T. J.-L., Fink, H. H., Makino, F., Otani, C., & Wamsteker, W. 1994, A&A, 285, 11 (W94)
Wanders, I., et al. 1995, ApJ, 453, L87
White, R. J., & Peterson, B. M. 1994, PASP, 106, 879